Acta Oceanol. Sin., 2021, Vol. 40, No. 3, P. 18–26
https://doi.org/10.1007/s13131-021-1714-5
http://www.hyxb.org.cn
E-mail: hyxbe@263.net

Submesoscale eddies in the East China Sea detected from SAR images

Yuxiang Ji[1, 5], Guangjun Xu[2, 3], Changming Dong[1, 3]*, Jingsong Yang[4], Changshui Xia[5]

[1] School of Marine Sciences, Nanjing University of Information Science and Technology, Nanjing 210044, China

[2] Ocean Remote Sensing and Information Technology Laboratory, Guangdong Ocean University, Zhanjiang 524088, China

[3] Southern Marine Science and Engineering Guangdong Laboratory (Zhuhai), Zhuhai 519000, China

[4] Second Institute of Oceanography, Ministry of Natural Resources, Hangzhou 310012, China

[5] First Institute of Oceanography, Ministry of Natural Resources, Qingdao 266061, China

Received 29 January 2020; accepted 12 April 2020

Abstract

Seven-year (2005–2011) Synthetic Aperture Radar (SAR) images are applied to study oceanic eddies in the East China Sea. It is found that most of these eddies detected from the SAR images are less than 10 km, which are submesoscale eddies. Seasonal differences are evident in the distribution of eddies, with the highest and the lowest number of eddies noted in summer and winter, respectively. Since slick streaks in SAR images look dark, an eddy identified due to the slicks is referred to as “black eddy”. As a result of wave-current interactions in the zones of current shear, it can be seen that an eddy exhibits a bright curve, the eddy is called “white eddy”. During the seven years, 95 black eddies and 50 white eddies are identified in the study area. Black eddies are found in the whole study area while white eddies are mainly distributed in the vicinity of the Kuroshio Current. This study suggests that the distribution of the white eddy is denser around the Kuroshio because of the strong shear in the Kuroshio region. In terms of the eddy sizes, white eddies are generally smaller than black eddies.

Key words: submesoscale, ocean eddy, Synthetic Aperture Radar, East China Sea

Citation: Ji Yuxiang, Xu Guangjun, Dong Changming, Yang Jingsong, Xia Changshui. 2021. Submesoscale eddies in the East China Sea detected from SAR images. Acta Oceanologica Sinica, 40(3): 18–26, doi: 10.1007/s13131-021-1714-5

1 Introduction

Ocean eddies are common phenomena in the ocean. They are widely distributed in the global ocean and marginal seas. They are important parts of the marine system and have great impacts on the marine environment, which can induce upwelling and downwelling, modulating the temperature and salt compositions of seawater (Dong et al., 2011). They also play an important role in the transport of energy and chemical substances, and thus affect the ocean circulation structure and the distribution of water masses and marine organisms (Chelton et al., 2007).

Ocean eddies have been an important field of research among oceanographers since their discovery. Previously, ocean eddies have been studied using different data, such as sea level anomaly (SLA) (Wang et al., 2003; Jia and Liu, 2004; Yuan et al., 2006, 2007; Chelton et al., 2011; Liu et al., 2012) and sea surface temperature (SST) (Dong et al., 2011). However, the spatial resolutions of these data can only resolve mesoscale eddies, which limit the capability of submesoscale eddy detection.

Synthetic Aperture Radar (SAR) is an active microwave imaging radar, carrying high resolution images. It measures amplitudes and time phases of backscattering signals on the sea surface and generates a backscattering intensified image after processing. SAR images have several advantages: wide range; high-resolution; all-day and all-weather; and can penetrate through the cloud to observe the sea surface. DiGiacomo and Holt (2001) use ERS-1/2 (European Remote-Sensing Satellite) satellite images from 1992 to 1998 to study small-scale eddies in the South California Bay. They find that these eddies are mainly cyclonic with diameters less than 50 km and more than 70% are less than 10 km. SAR images have been used in the study of ocean vortex trains (OVT) in the Luzon Strait and island-induced ocean vortex trains (IOVTs) Kuroshio region southeast of Taiwan Island (e.g., Zheng et al., 2008; Zheng and Zheng, 2014; Zheng, 2017). They find that both vortex and vortex train in the Luzon Strait carry submesoscale natures and the variability of IOVTs in the Kuroshio region has a distinct seasonality. It has been suggested that small-scale (radius less than 20 km) eddies can be identified from SAR images (Fu and Holt, 1983; Johannessen et al., 1987, 1993, 1996; Liu et al., 1994; Nilsson and Tildesley, 1995; Gade et al., 1998; Munk et al., 2000; Eldevik and Dysthe, 2002; Font et al., 2002; Xu et al., 2015; Du et al., 2019). The ability of SAR to capture fine-scale details of the sea surface features makes it possible to observe submesoscale eddies, thus making SAR an effective approach for submesoscale eddy observation.

According to the imaging mechanism, oceanic eddies can be

Foundation item: The National Key Research and Development Program of China under contract Nos 2016YFA0601803 and 2017YFA0604100; the National Natural Science Foundation of China under contract Nos 41476022, 41490643 and 41706008; the China Ocean Mineral Resources R&D Association under contract Nos DY135-E2-2-02 and DY135-E2-3-01.

*Corresponding author, E-mail: cmdong@nuist.edu.cn classified into two types: black eddies and white eddies (Karimova, 2012). Since slick streaks in SAR images look dark, eddies identified due to the slicks are referred to as “black eddies”. As a result of wave-current interactions in the zones of current shear, it can be seen that the eddy exhibits a bright curve, these eddies are called “white eddies”. Karimova (2012) study small-scale eddies in the Baltic Sea, Black Sea and Caspian Sea using Envisat (Environmental Satellite) ASAR (Advanced Synthetic Aperture Radar) and ERS-2 SAR images from 2009 to 2010. They find that 98% of the detected eddies are cyclonic, with a diameter ranging between 1 km to 75 km, of which 99% are 1–20 km in diameter, and 71% are black eddies (mainly in summer, spring and autumn), while the seasonal distribution of the white eddies is not very obvious.

The detection of ocean eddies using SAR images has been widely applied in many sea areas around the world, but the study of ocean eddies using the SAR images in the East China Sea is still lacking. In this paper, the study area is 20°–40°N, 115°–135°E, images from the Envisat ASAR are used to analyze the spatial-temporal distribution characteristics of the eddies in the East China Sea.

The present paper is organized as follows: Section 2 introduces data and methods used in the present study; the results obtained in this study are presented in Section 3; Sections 4 and 5 are discussions and conclusions, respectively.

2 Observational data and methods

2.1 *Observational data*

SAR images from the Envisat satellite are used in the present study. The Envisat is the European Space Agency’s advanced polar orbit observation satellite. It was launched on March 1, 2002 and ended its mission on April 8, 2012. It is equipped with the ASAR, which produces high-quality and high-resolution images of oceans, coasts, polar ice caps and land, enabling the study of changes in the ocean. Envisat’s ASAR is operated in the C-band and has the characteristic of multi-polarization, multi-mode and wide swath. It mainly has five modes: IM (image) mode, AP (alternating polarisation) mode, WS (wide swath) mode, GM (global monitoring) mode, and WV (wave) mode. In this paper, images from AP, IM and WS modes from 2005 to 2011 are used to identify ocean eddies in the study area. The swath width of the image from the AP or IM mode is 100 km and its resolution is 30 m. The swath width of the image from the WS mode is 400 km and its resolution is 150 m.

In addition, the (1/4)°×(1/4)° sea level anomaly (SLA) and geostrophic current speed data from 2005 to 2011 provided by the Copernicus Marine Environment Monitoring Service (CMEMS) and the (1/12)°×(1/12)° global sea surface temperature (SST) data provided by HYCOM are used to compare with the eddies identified in the SAR images. Monthly mean sea surface wind speed data provided by National Oceanic and Atmospheric Administration (NOAA) on a (1/24)°×(1/24)° grid is used to analyze the relationship between the seasonal distribution of the eddy and the wind speed.

2.2 *Methods*

2.2.1 *Eddy detection methods*

In this study we apply the eddy detection method developed by Xu et al. (2015) to the SAR images collected in the East China Sea as we are aware of that the artificial intelligent (AI) method is used in the eddy detection from SAR images (Du et al., 2019).

In this paper, the boundary of an eddy is defined as the outermost dark or bright curve (black circle in Fig. 1a). The point at which the stripes or curves meet is defined as the center of the eddy. Eight straight lines in eight directions are drawn passing through the center of the eddy to the boundary of the eddy (yellow lines in Fig. 1a). The average length of the straight lines is taken as the diameter of the eddy. The polarity of the eddy is defined by the rotation direction of the spiral. In the northern hemisphere, a cyclonic eddy has a counter-clockwise rotation and an anticyclonic eddy has a clockwise rotation. Using the above definition, we identify the eddies in the SAR images, determine their position, size and polarity, and conduct a statistical analysis of these eddy data.

2.2.2 *Detection of black and white eddies*

As Karimova (2012) points out, two types of eddies (black and white) can be identified from the SAR images. One is that the natural slicks move with the eddy on the sea surface showing a spiral of light and dark stripes, and it is called as “black eddy”. The other type of eddies is due to the shear of ocean currents produced by eddies, the high backscattering caused by wave-current interaction in the shear area makes the eddy look like bright curved stripes on SAR images and it is called “white eddy”. Figures 1b and c show one black eddy (left panel) and one white eddy (right panel). The black and white eddies are identified from the SAR images we collect in the East China Sea.

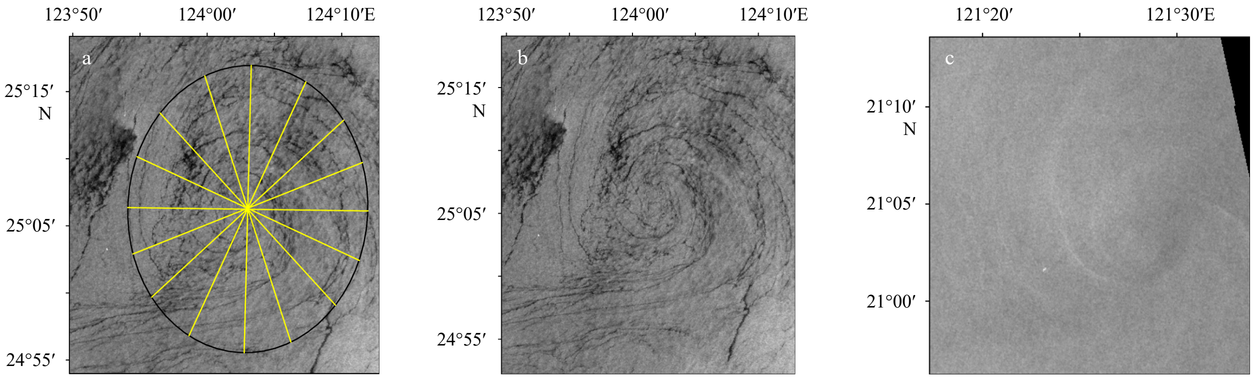

Fig. 1. An eddy identified by SAR image (a), black eddy (b, 2008/07/11 UTC 01:48), and white eddy (c, 2008/08/10 UTC 13:53) identified by the Envisat SAR. In a, the outer black ellipse is the eddy boundary; the aggregation point of black curves in the SAR image is the center of the eddy; the average length of eight yellow straight lines passing through the eddy center is the diameter.

3 Results

A total of 3 100 SAR images covering the East China Sea are collected and 104 images capturing one or more eddies are initially screened from these SAR images. The rate of the number of images including eddies to the total number of SAR images is similar to that suggested by Xu et al. (2015) in the oceanic areas near the Luzon Strait. Table 1 shows the temporal distribution of SAR images which include eddies. The analyses of these detected eddies are presented below.

3.1 *Characteristics of detected eddies*

In this paper, the size of an eddy is defined as the radius of the eddy. The histogram of the eddy radii is shown in Fig. 2. Most of the eddies' radii identified in the SAR images are less than 20 km; only 6 eddies with radii larger than 20 km. Eddies with radii less than 20 km account for 95.86%, and eddies with radii between 2–8 km account for 82.76%. According to McWilliams (2016), the submesoscale eddies are defined as those eddies with their radii less than the local first baroclinic deformation radius and larger than the turbulence mixing layer thickness. Based on Chelton et al. (1998), the first deformation radius in the East China Sea is about 20–50 km. Therefore, most of the eddies identified from the SAR images in the East China Sea are submesoscale.

Table 1. The temporal distribution of the number of SAR images (a total of 104) capturing eddies by season and year

Year	Number				
	Spring	Summer	Autumn	Winter	Total
2005	3	4	15	1	23
2006	0	3	0	0	3
2007	1	7	4	1	13
2008	5	12	1	8	26
2009	5	4	2	1	12
2010	2	5	2	0	9
2011	5	7	1	5	18
Total	21	42	25	16	104

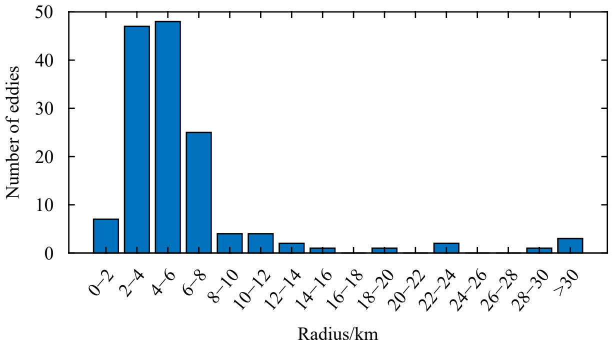

Fig. 2. The radius histogram of eddies identified in the SAR images in the East China Sea from 2005 to 2011. Most of the eddies identified in the SAR images are submesoscale eddies with radius less than 20 km. Most of the radius of the eddies is concentrated in the range of 0–10 km.

Figure 3 compares the distribution of black and white eddies radii. It can be seen that the radius of most black and white eddies is mainly concentrated in the range of 0–10 km. The range of 4–6 km records the highest number of black eddies while the highest number of white eddies is distributed in the range of 2–4 km. Almost all radii of white eddies are distributed within the range of 0–8 km, while the radii of black eddies are more widely distributed. This shows that the size of white eddies is generally smaller than that of black eddies, and more concentrated in the smaller scale.

In addition to the characteristics of the eddy radii, we find that the number of cyclonic eddies (128) is much larger than that of anticyclonic eddies (17) identified from SAR images. There are two reasons which can be applied for the interpretation of the phenomenon. The first reason is that the convergence of the cyclonic eddy is beneficial to the accumulation of natural slicks on the sea surface. The natural slicks limit the formation of microscale waves on the sea surface, which makes the region of eddies has a clear contrast with the surrounding rough sea surface, thus making the cyclonic eddies easier to be observed than anticyclonic eddies (Munk et al., 2000). Another reason is that the centrifugal instability of ocean current leads to the instability of the anticyclonic eddy. When the local Rossby number is large, it is difficult for the anticyclonic eddy to survive, resulting in more cyclonic than anticyclonic eddies (Dong et al., 2007).

3.2 *Spatial distribution of detected eddies*

3.2.1 *Overall spatial distribution of eddies*

A total of 145 eddies are identified in the 104 SAR images in the East China Sea. Their distribution is shown in Fig. 4. Eddies are observed over the whole East China Sea, and most of them are located along the coast of Fujian and Zhejiang Provinces, east and northeast of Taiwan Island. A few of them can be found in

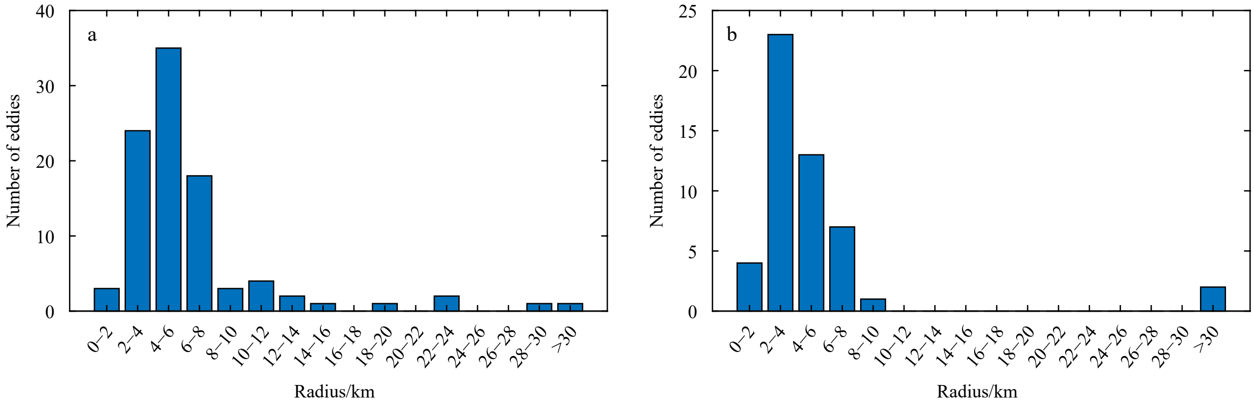

Fig. 3. The radius histograms of black (a) and white (b) eddies in the East China Sea. The radii of most black and white eddies are mainly concentrated in the range of 0–10 km and the radii of white eddies are more concentrated in the smaller scale than the radii of black eddies.

the eastern part of the Korean Peninsula.

3.2.2 *Spatial distribution of black and white eddies*

Of the 145 eddies identified from 2005 to 2011, 95 are black eddies and 50 are white eddies (Fig. 5). In addition, most of the eddies, for both black and white eddies, are cyclonic, which is consistent with previous studies (DiGiacomo and Holt, 2001; Font et al., 2002; Xu et al., 2015).

Figure 6 shows the spatial distribution of black and white eddies during the 7-year period. It shows that the black eddies are distributed over the whole area, while the white eddies are mainly concentrated in the Kuroshio and its adjacent areas. Few eddies are observed over the rest of the area. To understand the distribution of the white eddies around the Kuroshio area, we calculate the current shears from the HYCOM model data. Figure 7 shows the spatial distributions of both the shear deformation rate (ξ) from the average current data from 2005 to 2011 and white eddies. The shear deformation rate of surface currents is defined as (Kim, 2010)

$$\xi = \frac{\partial v}{\partial x} + \frac{\partial u}{\partial y},$$

where u and v are the velocity along the zonal (x-axis) and meridional (y-axis) directions respectively. It can be seen from Fig. 7 that more white eddies are presented in the area with strong current shears. The formation mechanism of white eddies is the high backscattering of wave-current interaction in the shear region

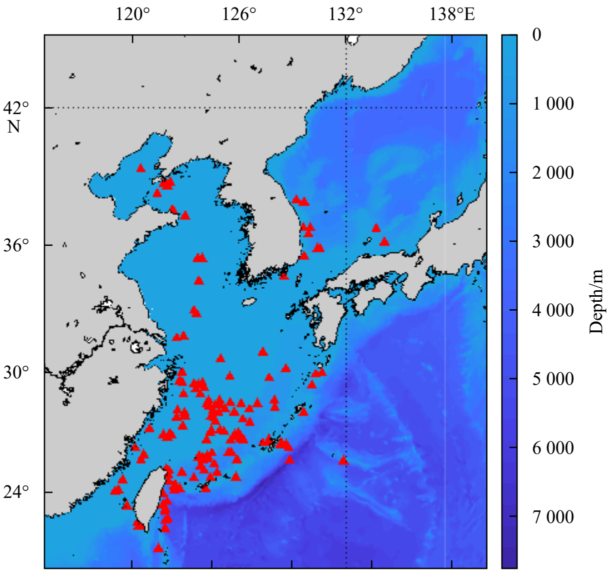

Fig. 4. Spatial distribution of eddies in the East China Sea. The red triangles represent the center locations of the eddies. The background color is bathymetry (m). The data is derived from gridded bathymetry data provided by the General Bathymetric Chart of the Oceans (GEBCO).

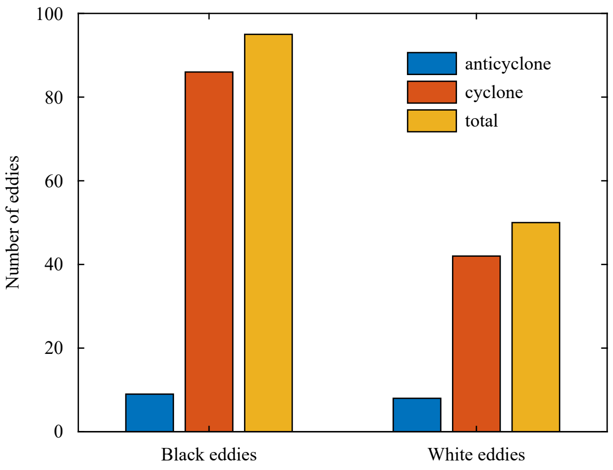

Fig. 5. Comparison between the numbers of black eddies and white eddies. The blue, orange and yellow bars represent the number of anticyclonic eddies, cyclonic eddies and total number of eddies, respectively.

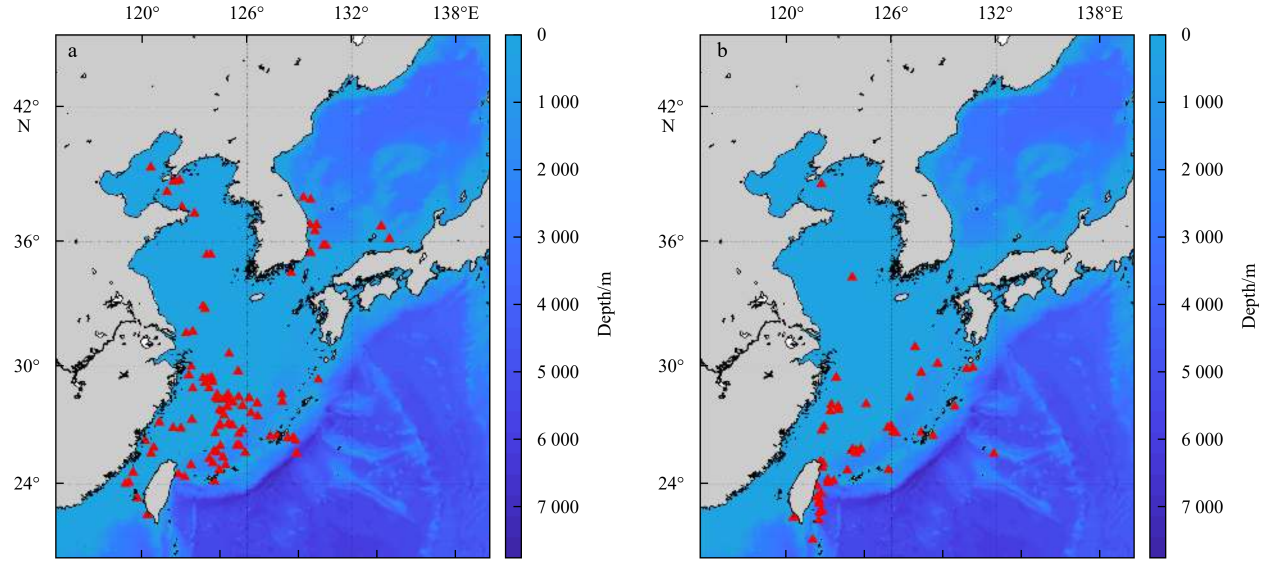

Fig. 6. Spatial distribution of black eddies (a) and white eddies (b). The red triangles represent the center locations of the eddies. The background color is bathymetry (m). The black eddies are distributed over the whole area while the white eddies are mainly concentrated in the Kuroshio and its adjacent areas.

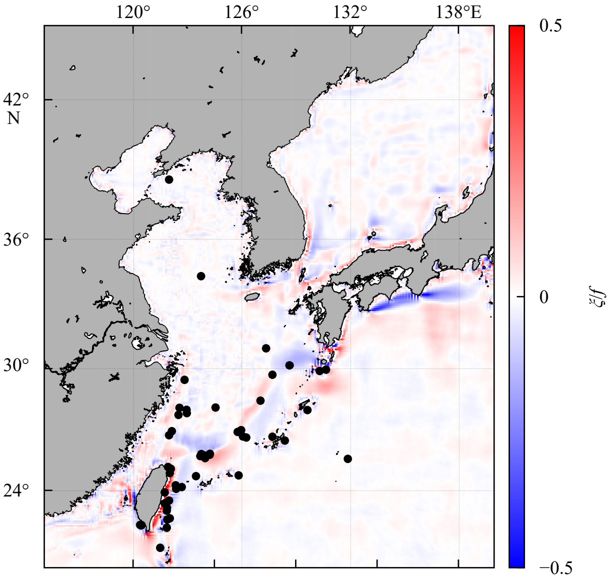

Fig. 7. The spatial distributions of the shear deformation rate (ξ/f) of sea surface current and white eddies. The background color is the shear deformation rate and black points denote locations of eddies. Eddies are mostly distributed in areas of large shear deformation rates.

(Karimova, 2012). Therefore, more white eddies are identified in the Kuroshio and its surrounding areas with strong shear.

3.3 *Temporal distribution of detected eddies*

3.3.1 *Interannual distribution*

Figure 8 shows the annual number of eddies from 2005 to 2011. An average of 21.7 eddies per year are identified, of which 18.3 are cyclonic eddies and 3.4 are anticyclonic eddies. The largest number of eddies (45) is identified in 2008 and the smallest number (10) is recorded in 2006. The number of eddies appearing in other years ranges from 15 to 20. In order to eliminate the influence of the different number of SAR images available per year, we divide the number of eddies found in one year by the number of SAR images available for the corresponding year (Fig. 9). According to the normalization by the number of the SAR images, the largest number of eddies is identified in 2006. More than three eddies can be identified in each SAR image in 2006. The least number of eddies is identified in 2005, with an average of only 0.70 eddies. The number of eddies identified in each SAR image in the other years ranges from 1 to 2.

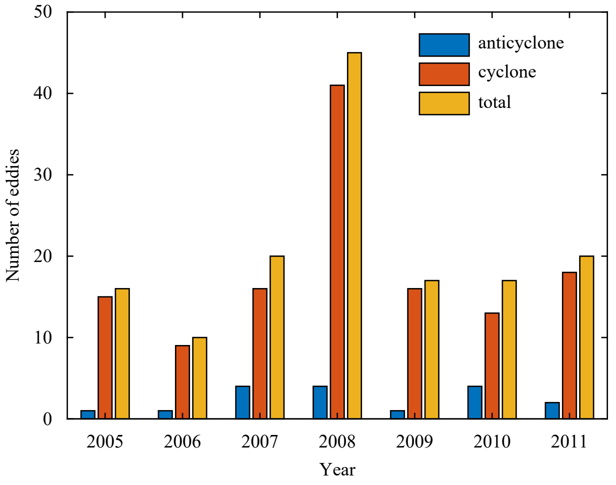

Fig. 8. Annual distribution of the number of eddies in 2005–2011. The blue, orange and yellow bars represent the number of anticyclonic eddies, cyclonic eddies and total number of eddies, respectively. The largest number of eddies is identified in 2008 and the smallest number is recorded in 2006. The number of eddies identified in the other years ranges from 15 to 20.

3.3.2 *Seasonal distribution*

Figure 10 shows the seasonal distribution of eddies in the East China Sea identified in SAR images. The seasonal variation is

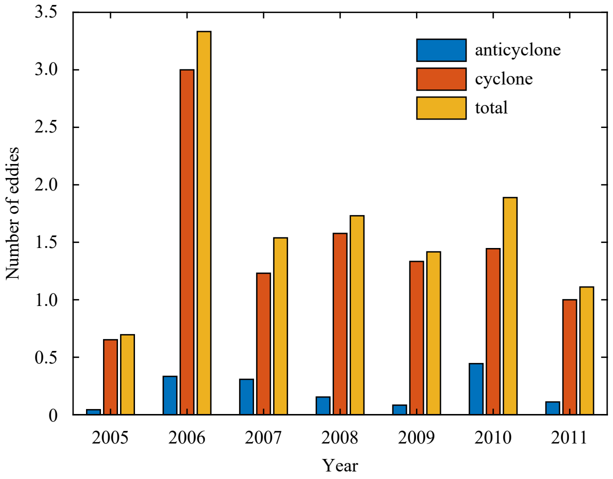

Fig. 9. Annual distribution of the number of eddies identified in each SAR image which can be used for eddy detection. The blue, orange and yellow bars represent the number of anticyclonic eddies, cyclonic eddies and total number of eddies, respectively. In 2006, the number of eddies identified in each SAR image is the largest (3.33) and the lowest (0.70) in 2005. In the other years, the number of eddies identified in each SAR image ranges from 1 to 2.

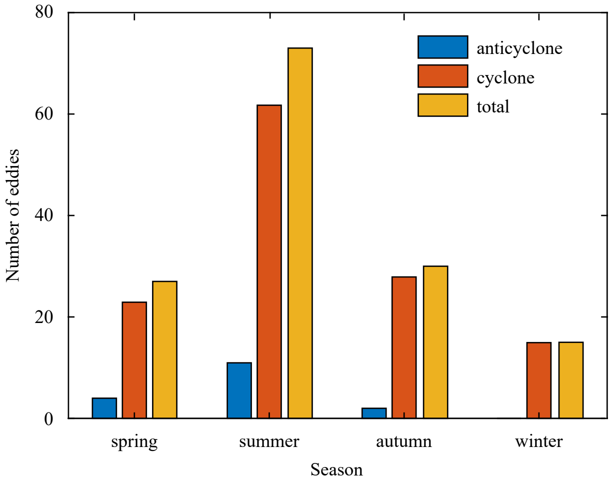

Fig. 10. Seasonal distribution of the number of eddies in the East China Sea. The blue, orange and yellow bars represent the number of anticyclonic eddies, cyclonic eddies and total number of eddies, respectively.

evident in the distribution of the eddy number. The number of eddies is the largest in summer, followed by spring and autumn, and the lowest in winter. In addition, cyclonic eddies account for the majority of eddies in any season. The number of anticyclonic eddies is very small and no anticyclonic eddies are identified in winter. The seasonal distribution of the number of cyclonic and anticyclonic eddies is the highest in summer, followed by spring and autumn, and the lowest in winter. In order to eliminate the difference in the number of SAR images available for the different seasons, we divide the number of eddies identified in each season by the corresponding number of SAR images available for that season (Fig. 11). It is shown that seasonal differences still exist; the number of eddies is still highest in summer and the lowest in winter. In summer, an average of 1.74 eddies are identified in each SAR image, while only 0.81 eddies can be identified in winter. The number of eddies identified in each SAR image in spring and autumn are almost similar with a difference of only 0.02.

The reason for the seasonal variation can be attributed to the seasonal changes of the surface wind. Figure 12 shows the seasonally averaged sea surface wind speed in the study area from 2005 to 2011. The wind speed is the highest in winter (in most areas the wind is above 8 m/s), followed by autumn and spring, while the average wind speed in summer is the lowest. By comparing the seasonal distribution of the mean wind speed and the eddy number, we find that the average wind speed is the lowest in summer while the number of eddies is the highest in that season. On the contrary, the average wind speed in winter is the

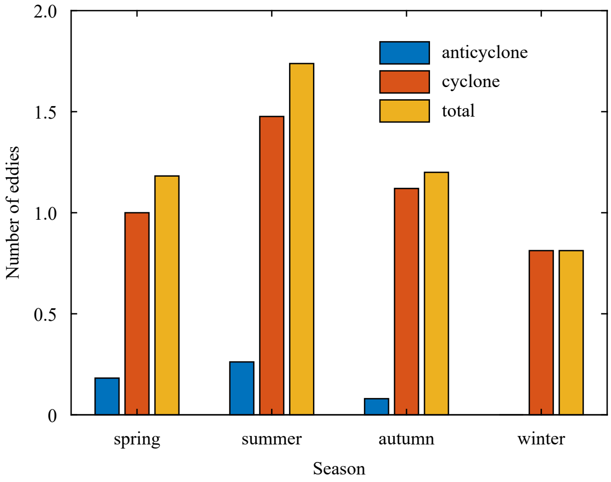

Fig. 11. Seasonal distribution of the number of eddies identified in each SAR image. The blue, orange and yellow bars represent the number of anticyclonic eddies, cyclonic eddies and total number of eddies, respectively.

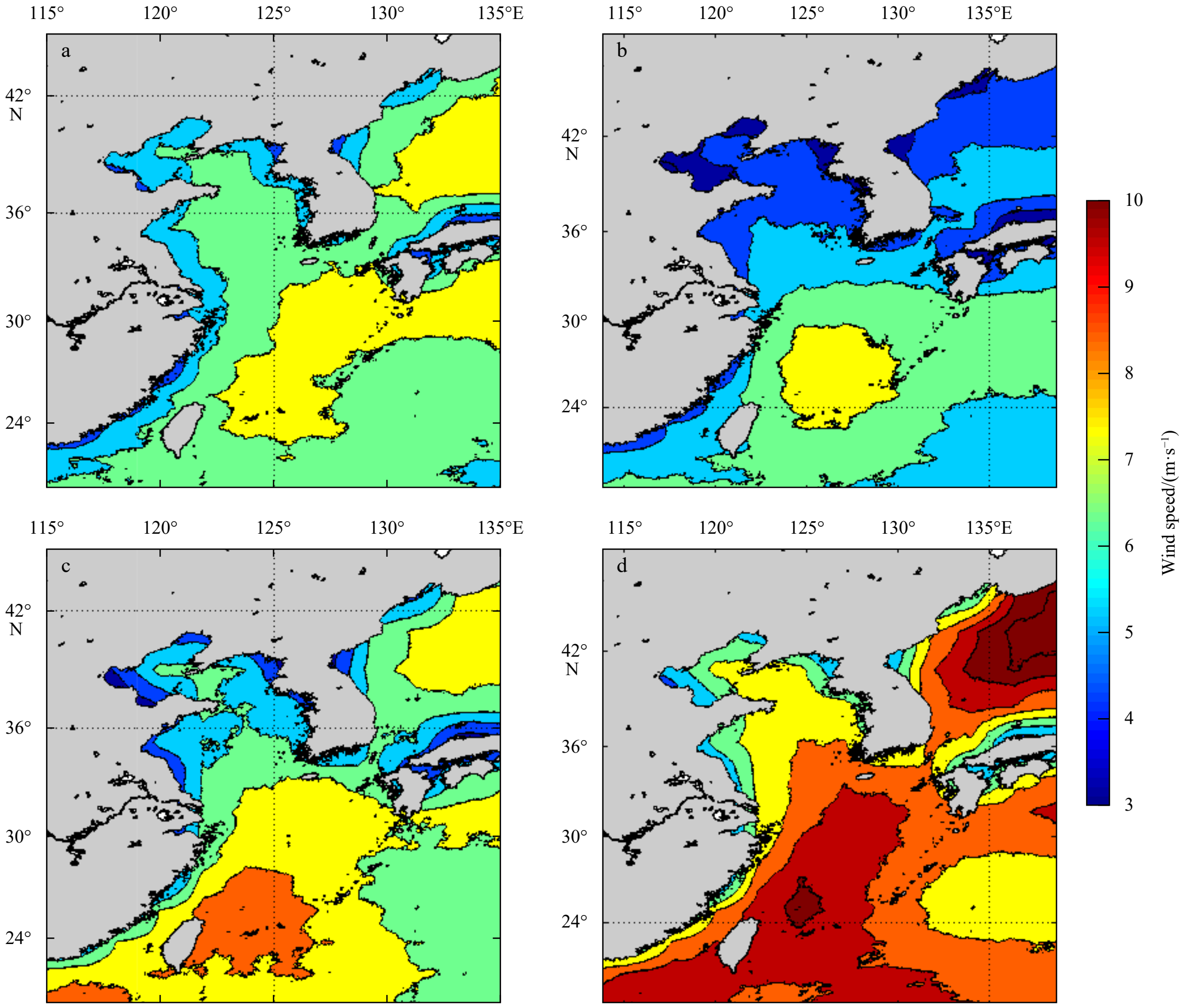

Fig. 12. Seasonal average of 10-m wind speeds from 2005 to 2011 for spring (a), summer (b), autumn (c), and winter (d).

highest while the number of eddies is the lowest. In summer, the low wind speed causes small-scale wave on the sea surface, producing weak backscattering. For white eddies, the sea surface roughness is larger than that of the surrounding sea surface, and it appears brighter on the SAR images. For black eddies, the roughness is smaller than that of the surrounding sea surface, and it appears darker on the SAR images. Eddies are identified from the contrasting bright and dark stripes. However, the high wind speed in winter makes the whole sea surface too rough, so that the whole sea surface appears bright on the SAR images. Eddies are difficult to be identified in such images. In addition, Zheng (2017) point out that natural slicks and low wind speed are important conditions for eddy detection. Espedal et al. (1998) study the dependence of natural slicks on wind speed by using ERS 1/2 SAR images. They note that up to 40% natural slicks coverage was found for 2.5 m/s wind speeds, but only 5% for 5–10 m/s. Espedal (1999) find that under the influence of the breaking waves, natural slicks disappear at high wind speed. Therefore, those black eddies are not well visible because high wind speed leads to less natural slicks accumulated on the sea surface. There are little differences between spring and autumn wind speed, thus little difference is presented between the sea surface roughness in these two seasons. Therefore, the number of eddies identified in the two seasons are almost the same.

To examine the effect of the surface wind speed on the shapes of eddies, we used eddy deformation rate to represent forms (shapes) of eddies, the deformation rate is defined as

$$\lambda = \frac{r_1 - r_2}{r_1 + r_2},$$

where λ represents the deformation rate, r_1 and r_2 represent the longest and shortest axes, respectively.

Daily sea surface wind speed data provided by NOAA on a (1/24)°×(1/24)° grid is used to analyze the effect of sea surface wind speeds on forms of eddies. Wind data at twenty-five grid points around each eddy center are averaged to yield wind intensity over the eddy. The correlation coefficient between wind speed and eddy deformation rate is –0.04 and it shows that there is no significant correlation between them. Therefore, the surface winds are not dominate effect on the forms of eddies in this area.

4 Discussion

Geostrophic current speed, SLA and SST data are used to compared with the SAR images data to validate the eddies identified in the SAR images.

As an example, an eddy shown in Fig. 13a is a cyclonic eddy identified from an Envisat SAR image in the eastern Bohai Sea on September 16, 2009. The center point of the eddy is (38.29°N, 121.39°E). The geostrophic current field on September 16, 2009 from CMEMS (Fig. 13b) shows that the center point of the eddy is (38.37°N, 121.03°E). The low SLA and cold SST are presented in the area of the cyclonic eddy (Figs 13c and d). By comparing these four kinds of data, it is found that eddies identified in the

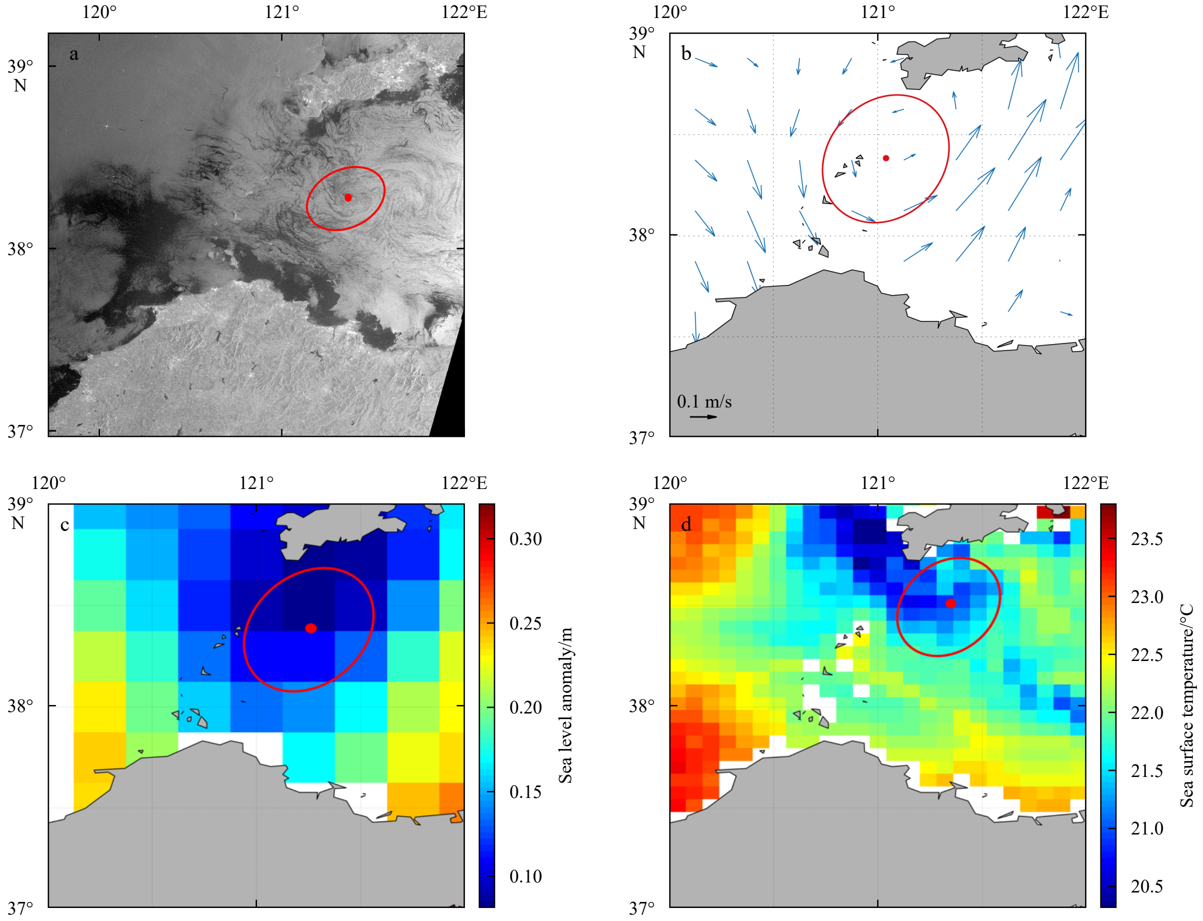

Fig. 13. A cyclonic eddy identified by the SAR image (a), geostrophic current field (b), sea level anomaly (c), and sea surface temperature (d) in the Bohai Sea on September 16, 2009.

SAR images are also confirmed in the geostrophic current, SLA and SST data. Due to the spatial resolution limitation of these three types of observational data, eddies with radii less than 20 km cannot be identified. However, the high spatial resolution of SAR images allows small-scale ocean eddies to be identified. Therefore, SAR images have more advantages than the SLA, geostrophic current and SST data in the observation of sub-mesoscale ocean phenomena.

5 Conclusions

In this study, 104 SAR images screened from 3 100 SAR images in the period from 2005 to 2011 are used to identify ocean eddies in the analysis of the spatial-temporal distribution, and their size distribution in the East China Sea. The following conclusions are reached:

(1) Most of the ocean eddies observed from SAR images are submesoscale and their radii are concentrated in the range of 2–8 km. The high spatial resolution of SAR images makes it easier to observe small-scale ocean phenomena, therefore, SAR is an effective means to study submesoscale eddies.

(2) Most of the eddies observed by SAR images are cyclonic eddies, accounting for 88.28% of the total, and only 11.72% are anticyclonic eddies.

(3) According to the different formation mechanism, the detected eddies can be classified into two types: black and white eddies. More black eddies are found than white eddies in the East China Sea. Black eddies are distributed throughout the East China Sea, while white eddies are mostly distributed in the Kuroshio region. This is mainly due to the strong shear in the Kuroshio region.

(4) Seasonal variation is evident in the distribution of the eddy number. The number of eddies observed in summer (winter) is significantly higher (lower) than that in other seasons.

References

Chelton D B, Deszoeke R A, Schlax M G, et al. 1998. Geographical variability of the first baroclinic Rossby radius of deformation. Journal of Physical Oceanography, 28(3): 433–460, doi: 10.1175/1520-0485(1998)028<0433:GVOTFB>2.0.CO;2

Chelton D B, Schlax M G, Samelson R M. 2011. Global observations of nonlinear mesoscale eddies. Progress in Oceanography, 91(2): 167–216, doi: 10.1016/j.pocean.2011.01.002

Chelton D B, Schlax M G, Samelson R M, et al. 2007. Global observations of large oceanic eddies. Geophysical Research Letters, 34(15): L15606

DiGiacomo P M, Holt B. 2001. Satellite observations of small coastal ocean eddies in the Southern California Bight. Journal of Geophysical Research: Oceans, 106(C10): 22521–22543, doi: 10.1029/2000JC000728

Dong Changming, McWilliams J C, Shchepetkin A F. 2007. Island wakes in deep water. Journal of Physical Oceanography, 37(4): 962–981, doi: 10.1175/JPO3047.1

Dong Changming, Nencioli F, Liu Yu, et al. 2011. An automated approach to detect oceanic eddies from satellite remotely sensed sea surface temperature data. IEEE Geoscience and Remote Sensing Letters, 8(6): 1055–1059, doi: 10.1109/LGRS.2011.2155029

Du Yanling, Song Wei, He Qi, et al. 2019. Deep learning with multi-scale feature fusion in remote sensing for automatic oceanic eddy detection. Information Fusion, 49: 89–99, doi: 10.1016/j.inffus.2018.09.006

Eldevik T, Dysthe K B. 2002. Spiral eddies. Journal of Physical Oceanography, 32(3): 851–869, doi: 10.1175/1520-0485(2002)032<0851:SE>2.0.CO;2

Espedal H A. 1999. Satellite SAR oil spill detection using wind history information. International Journal of Remote Sensing, 20(1): 49–65, doi: 10.1080/014311699213596

Espedal H A, Johannessen O M, Johannessen J A, et al. 1998. COASTWATCH'95: ERS 1/2 SAR detection of natural film on the ocean surface. Journal of Geophysical Research: Oceans, 103(C11): 24969–24982, doi: 10.1029/98JC01660

Font J, Rousseau S, Shirasago B, et al. 2002. Mesoscale variability in the Alboran Sea: synthetic aperture radar imaging of frontal eddies. Journal of Geophysical Research: Oceans, 107(C6): 3059, doi: 10.1029/2001JC000835

Fu L L, Holt B. 1983. Some examples of detection of oceanic mesoscale eddies by the SEASAT synthetic-aperture radar. Journal of Geophysical Research: Oceans, 88(C3): 1844–1852, doi: 10.1029/JC088iC03p01844

Gade M, Alpers W, Huhnerfuss H, et al. 1998. Imaging of biogenic and anthropogenic ocean surface films by the multifrequency/multipolarization SIR-C/X-SAR. Journal of Geophysical Research: Oceans, 103(C9): 18851–18866, doi: 10.1029/97JC01915

Jia Yinglai, Liu Qinyu. 2004. Eddy shedding from the Kuroshio bend at Luzon strait. Journal of Oceanography, 60(6): 1063–1069, doi: 10.1007/s10872-005-0014-6

Johannessen J A, Johannessen O M, Svendsen E, et al. 1987. Mesoscale eddies in the Fram Strait marginal ice zone during the 1983 and 1984 Marginal Ice Zone Experiments. Journal of Geophysical Research: Oceans, 92(C7): 6754–6772, doi: 10.1029/JC092iC07p06754

Johannessen J A, Roed L P, Wahl T. 1993. Eddies detected in ERS-1 SAR images and simulated in reduced gravity model. International Journal of Remote Sensing, 14(11): 2203–2213, doi: 10.1080/01431169308954029

Johannessen J A, Shuchman R A, Digranes G, et al. 1996. Coastal ocean fronts and eddies imaged with ERS 1 synthetic aperture radar. Journal of Geophysical Research: Oceans, 101(C3): 6651–6667, doi: 10.1029/95JC02962

Karimova S. 2012. Spiral eddies in the Baltic, Black and Caspian seas as seen by satellite radar data. Advances in Space Research, 50(8): 1107–1124, doi: 10.1016/j.asr.2011.10.027

Kim S Y. 2010. Observations of submesoscale eddies using high-frequency radar-derived kinematic and dynamic quantities. Continental Shelf Research, 30(15): 1639–1655, doi: 10.1016/j.csr.2010.06.011

Liu Yu, Dong Changming, Guan Yuping, et al. 2012. Eddy analysis in the subtropical zonal band of the North Pacific Ocean. Deep Sea Research Part I: Oceanographic Research Papers, 68: 54–67, doi: 10.1016/j.dsr.2012.06.001

Liu A K, Peng C Y, Schumacher J D. 1994. Wave-current interaction study in the Gulf of Alaska for detection of eddies by synthetic aperture radar. Journal of Geophysical Research: Oceans, 99(C5): 10075–10085, doi: 10.1029/94JC00422

McWilliams J C. 2016. Submesoscale currents in the ocean. Proceedings of the Royal Society A: Mathematical, Physical and Engineering Sciences, 472(2189): 20160117, doi: 10.1098/rspa.2016.0117

Munk W, Armi L, Fischer K, et al. 2000. Spirals on the sea. Proceedings of the Royal Society A: Mathematical, Physical and Engineering Sciences, 456(1997): 1217–1280, doi: 10.1098/rspa.2000.0560

Nilsson C S, Tildesley P C. 1995. Imaging of oceanic features by ERS 1 synthetic aperture radar. Journal of Geophysical Research: Oceans, 100(C1): 953–967, doi: 10.1029/94JC02556

Wang Guihua, Su Jilan, Chu P C. 2003. Mesoscale eddies in the South China Sea observed with altimeter data. Geophysical Research Letters, 30(21): 2121, doi: 10.1029/2003GL018532

Xu Guangjun, Yang Jingsong, Dong Changming, et al. 2015. Statistical study of submesoscale eddies identified from synthetic aperture radar images in the Luzon Strait and adjacent seas. International Journal of Remote Sensing, 36(18): 4621–4631, doi: 10.1080/01431161.2015.1084431

Yuan Dongliang, Han Weiqing, Hu Dunxin. 2006. Surface Kuroshio path in the Luzon Strait area derived from satellite remote sensing data. Journal of Geophysical Research: Oceans, 111(C11): C11007, doi: 10.1029/2005JC003412

Yuan Dongliang, Han Weiqing, Hu Dunxin. 2007. Anti-cyclonic eddies northwest of Luzon in summer-fall observed by satellite altimeters. Geophysical Research Letters, 34(13): L13610

Zheng Quanan. 2017. Satellite SAR Detection of Sub-mesoscale Ocean Dynamic Processes. New Jersey London: World Scientific, 27-54

Zheng Quanan, Lin Hui, Meng Junmin, et al. 2008. Sub-mesoscale ocean vortex trains in the Luzon Strait. Journal of Geophysical Research: Oceans, 113(C4): C04032

Zheng Zhewen, Zheng Quanan. 2014. Variability of island-induced ocean vortex trains, in the Kuroshio region southeast of Taiwan Island. Continental Shelf Research, 81: 1–6, doi: 10.1016/j.csr.2014.02.010